AIAA JOURNAL
Vol. 44, No. 11, November 2006

Vortex Rings Generated by a Shrouded Hartmann–Sprenger Tube

Jack Wilson*
QSS Group, Inc., Cleveland, Ohio 44135
and
Mark P. Wernet† and Daniel E. Paxson‡
NASA Glenn Research Center, Cleveland, Ohio 44135

DOI: 10.2514/1.17560

The pulsed flow emitted from a shrouded Hartmann–Sprenger tube was sampled with high-frequency pressure transducers and with digital particle image velocimetry, and found to consist of a train of vortices. The mass flow was also monitored using an orifice meter. The tube and shroud lengths were altered to give four different operating frequencies. From the data, the radius, velocity, and circulation of the vortex rings were obtained. Each frequency corresponded to a different value of the slug length to diameter ratio. The slug length is the length of the volume of air emitted from the tube on each pulse. A modified version of the slug model of vortex ring formation was used to compare the observations with calculated values. Because the flow exit area is an annulus, vorticity is shed at both the inner and outer edge of the jet. However, the vorticity shed at the inner edge seems not to affect the circulation in the ring. The value of ring circulation obtained from digital particle image velocimetry did not agree with values calculated from the slug model, leading to a discrepancy between measured and calculated vortex ring velocity. The vortex ring radius, which does not depend on the circulation, does agree with a prediction from the slug model.

Nomenclature

a	=	radius of vortex ring core
c	=	speed of sound far from vortex ring
D	=	effective diameter of jet, $\sqrt{(D_s^2 - d_t^2)}$
D_s	=	inner diameter of shroud
d_t	=	outer diameter of resonance tube
$E(\varepsilon)$	=	dimensionless energy of vortex ring
F	=	formation number
f	=	frequency
$I(\varepsilon)$	=	dimensionless impulse of vortex ring
K	=	circulation
L	=	length of volume (slug) of air in each pulse
M	=	vortex core Mach number
$\dot{m}_{\text{jet}}$	=	time averaged mass flow rate of jet
m_{pulse}	=	mass of air in one pulse
P	=	vortex ring impulse
R	=	vortex ring radius
R_{pmin}	=	radial location of total pressure minima
r	=	distance along radius of vortex ring
r_0	=	radial limit of vorticity shed at inner annulus
s	=	axial separation between pressure probes
T	=	energy of vortex ring
t	=	time
U	=	characteristic jet velocity
U_1	=	average velocity defined in Eq. (A17)
U_2	=	average velocity defined in Eq. (A18)
$u(t)$	=	jet velocity as function of time
W	=	vortex ring velocity
x	=	axial separation between vortex rings
z	=	distance along axis of vortex ring
Γ	=	ratio of ring to slug circulation
ε	=	ratio a/R
ν	=	kinematic vorticity
ρ	=	density of air
τ	=	time between pulses $(1/f)$
τ_p	=	duration of square wave pulse
ω	=	vorticity

Presented as Paper 5163 at the 35th AIAA Fluid Dynamics Conference and Exhibit, Toronto, Canada, 6–9 June 2005; received 13 May 2005; revision received 10 July 2006; accepted for publication 13 July 2006.

*Senior Engineering Specialist, 21000 Brookpark Road. Associate Fellow AIAA

†Senior Research Engineer, 21000 Brookpark Road. Associate Fellow AIAA

‡Aerospace Research Engineer, 21000 Brookpark Road. Associate Fellow AIAA

I. Introduction

THERE is currently interest in investigating pulsed detonation engines for propulsion purposes. A review of research in this area has been given by Kailasanath [1]. Because the output from a pulsed detonation engine is obviously unsteady, this in turn has reinvigorated interest in unsteady ejectors [2–6]. In past experiments using a pulsejet [7] and a mechanically chopped flow [8], and more recently with a mechanically chopped flow [9], unsteady ejectors have been shown to be capable of achieving high values of thrust augmentation. The early experiments did not yield much information regarding the optimum design of such ejectors, and a need was felt for an unsteady jet which would be simpler to operate than a pulse detonation tube, but would be a useful source for experiments which could produce design data for unsteady ejectors. For this purpose, the unsteady jet should be capable of operating at different frequencies, be fully pulsed [10] (i.e., velocity goes to zero between pulses), and produce a pulse of fluid led by a shock wave to mimic a detonation wave. Mechanical chopping is obviously an easy technique for varying frequency, but due to the finite opening time of the chopper, the resulting pulse usually has a long rise time. Pulsejets produce high-speed jets, but changing frequency is not simple. Consideration was given instead to the use of a Hartmann–Sprenger tube. This is a device which, without any moving parts, transforms a steady flow into a pulsating flow. The Hartmann–Sprenger tube, formerly called a resonance tube, was discovered by Hartmann and Trolle [11] in 1922. Originally it consisted of a converging nozzle, producing an underexpanded supersonic jet, blowing into a closed tube situated on the axis of the jet. A shock will form in front of the tube, and if this shock is in a region of shock instability [12], i.e., Mach number decreasing with distance, oscillations will occur in which the tube

alternately fills with air, swallowing the jet, and then empties while deflecting the jet from the tube [13]. These oscillations have generated pressure amplitudes of 6 atm[13], intense sound over 40 dB [14], and temperatures as high as 900 K [15], and, using a vacuum insulated tube, 1000 K [16]. Applications of Hartmann–Sprenger tubes, in addition to being used as sirens, include fog dispersal and ultrasonic drying [14], explosive initiation [12], and proposals for improved mixing for scramjet combustion [17], and as flow control actuators [18]. Brocher [19] has shown that even a correctly expanded jet directed into a tube can oscillate, provided a needle is mounted on the axis of the nozzle. This geometry is shown as the nozzle and resonance tube of Fig. 1. Because there are now no unstable regions, the sensitivity of the tube position is reduced, and high pressures can be generated. Roughly speaking, the pressure inside the tube, at the closed end, alternates between the external pressure and the stagnation pressure of the driving jet. Thus this version of a Hartmann–Sprenger tube seemed a likely source for a strongly pulsed jet. To create a directed jet, a cylindrical shroud was placed around the nozzle and tube, concentrating the flow into a constant area annular region aligned with the tube axis. Brocher and Pinna [20] have previously used a diverging horn around a Hartmann–Sprenger tube in a similar manner, but their objective was to amplify the acoustic output, and no indication of the velocity field was given. Kastner and Samimy [18] put a shield around the region between nozzle exit and tube entrance, with an opening in it to allow exhaust egress. They imaged the exhaust flow using a sheet laser probe and acetone seeding, and observed wavy structures in the flow. This flow was orthogonal to the axis of the nozzle and tube. Thompson [21] used timed shadowgraphs to observe the flow between the nozzle and the entrance to the tube for an unshielded Hartmann–Sprenger tube, and clearly saw that there are definitely two phases; in the inflow phase, when the jet is filling the tube, there is no external flow, and there is a strong external flow when the tube is emptying. Thus the exhaust flow is indeed a pulsed flow in which the flow cuts off between pulses, and might be appropriate for generating a fully pulsed jet. If insight into unsteady thrust augmentation is to be gained, the properties of the driving jet should be known. This work was performed to establish the properties of the flow from the shrouded Hartmann–Sprenger tube. It is believed that this is the first time, other than the work of Brocher and Pinna [20], that a shrouded Hartman–Sprenger tube has been used to produce an axially directed, pulsed flow.

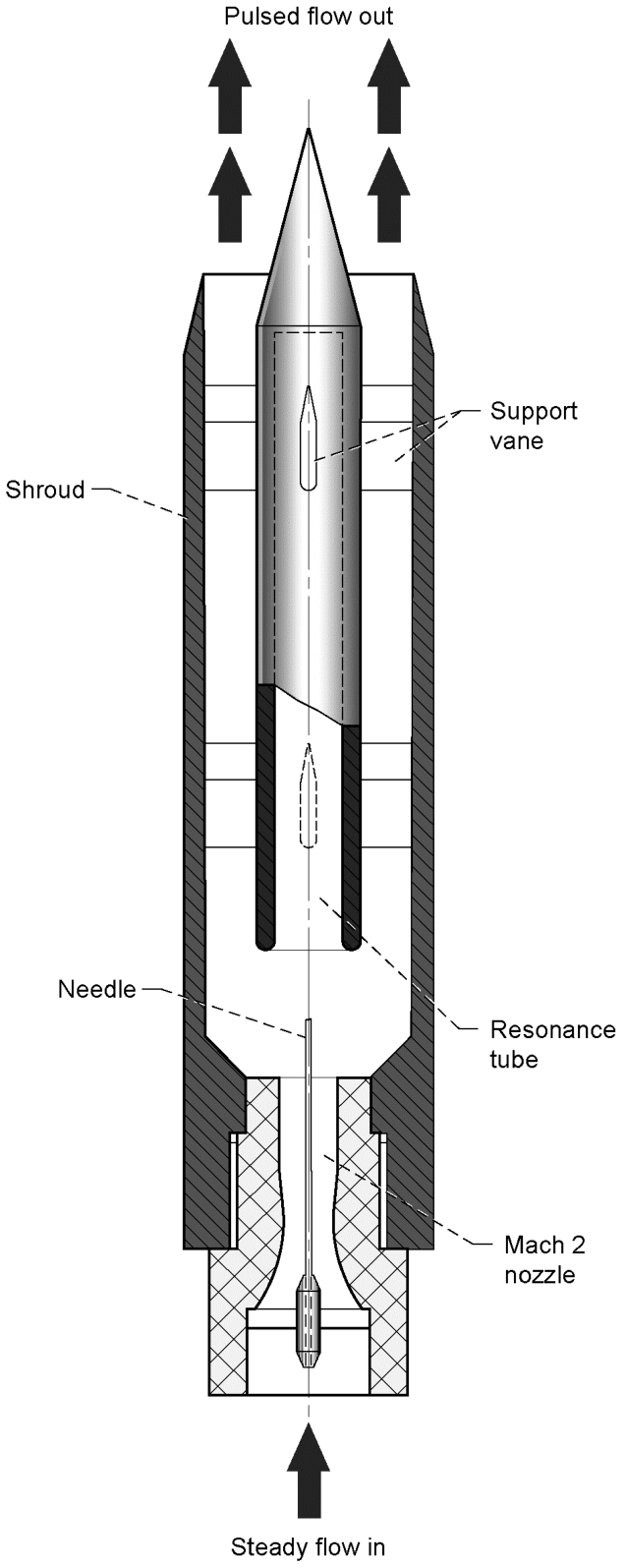

Fig. 1 Schematic drawing of the shrouded Hartmann–Sprenger tube.

It has been shown previously that a shock wave emerging from the open end of a shock tube produces a vortex ring (Payman and Shepherd [22], Elder and deHaas [23], Das et al. [24]). Thus it seems possible that the impulsively created flow from the shrouded Hartmann–Sprenger tube will also contain vortex rings. To confirm this, it is necessary to show that the flow contains reasonably coherent vortical structures, with the characteristic properties of vortex rings [25], namely R, W, and K_{ring} having reasonable values, i.e., consistent with values in the literature for similar conditions. Most studies of vortex rings have used a single pulse of water propelled into a tank of water by a piston [25–31], although there have also been studies in air [32,33], In these studies, attempts to relate the properties of the initial jet of fluid to those of the vortex rings produced, have resulted in the so-called slug model [25,29,34,35]. In this model, the values of R, a, and K_{ring} are found by balancing the impulse and energy of the vortex ring with those of the slug of fluid emitted from the source (see appendix for details). For a constant source velocity, the circulation is assumed to be produced by the boundary layer at the outer edge of the jet flow, with a value of $UL/2$. In a very careful set of experiments, Didden [25] showed that there are other contributions to the circulation, namely, a negative vorticity in the boundary layer of entrained fluid in the flow external to the nozzle, a positive vorticity from the fact that the maximum flow velocity in the jet has a higher velocity than the average value U due to the boundary layer displacement effect, increasing as time increases, and the starting flow around the nozzle edge creates a flow velocity greater than U near the edge, resulting in a large positive vorticity into the vortex ring. He showed that the resulting ring circulation is greater than $UL/2$ for his pulses. Using Didden's correction to the vorticity, Wiegand and Gharib [36] found good agreement between measurements of vortex ring circulation and calculated values, for $L/D < 0.68$. Further discussion of the relationship between slug and ring circulation can be found in the review article by Shariff and Leonard [37].

An important contribution to the understanding of vortex ring formation was provided by Gharib et al. [38], who found that a slug will transform into a vortex ring alone, provided that L/D is less than

a value called the formation number, F, and into a vortex ring followed by a trailing jet if $L/D > F$. They found that F is approximately 4. Subsequent work [39,40], has shown that F may not be a universal number, but may depend on the velocity program (i.e., the temporal variation of velocity) of the generating flow.

The present work differs from most prior work in several respects. First, the orifice which produces the jet is an annulus rather than a circle, and secondly, it is a train of pulses instead of a single pulse. The annulus affects the flow in two ways. The shear layer will be produced at the inner diameter of the outer tube, which is larger than the effective diameter for calculating the flow area. Also, because the flow emerges from an annulus, one could argue that a quantity of circulation of the order of $UL/2$ is produced at the outer diameter of the flow, and a quantity of equal magnitude, but opposite sign, is produced at the inner diameter. These could cancel each other, so that no vortex ring will result. However, as pointed out by a reviewer, because the vorticity from the inner diameter has the opposite sign to that produced at the outer diameter, its self-induced velocity will tend to carry it upstream, separating it from the primary vortex ring which travels downstream. Moreover, the inner vorticity is close to the centerline, and will dissipate by diffusion across the centerline. Thus a vortex ring should be produced.

The thrust of a jet consisting of a train of pulses has been studied by Krueger and Gharib [41], who found that the thrust was optimized when the value of L/D is close to the formation number, but that the velocity of the individual rings is not changed from the value for an isolated ring as a consequence of velocity induced by neighboring rings provided $x/R > 3$, a criterion derived by Weihs [42]. However, the rings do interact with each other for values of $z/D > 4$, with a tendency for rings to move off-axis, and could break up as the duty cycle approaches unity. Moreover, an additional effect found for pulses with $L/D > F$ is that vorticity from the trailing jet of the preceding pulse could affect the propagation of the vortex rings.

In this study, the flow exiting a shrouded Hartmann–Sprenger tube was probed with high-frequency pressure transducers, and found to be a train of periodic structures, each containing low pressure regions. The probes located the radius of the low pressure regions, and were also used to measure the velocities of the structures, as well as the velocity of the flow at the exit plane of the Hartmann–Sprenger tube. In addition, digital particle image velocimetry was used to map the velocity and vorticity distributions. The measurements are compared with calculations from the slug model, and from formulae of other workers.

II. Experimental Apparatus

A. Pulsed Jet Source

The Hartmann–Sprenger, or resonance, tube consists of a steady, sonic or supersonic jet, which is flowing into a closed tube. Under certain conditions, a periodic cycle is established in which the jet first fills the tube, then a hammer shock inside the tube empties the tube, deflecting the jet from the tube in the process. When the tube pressure has fallen sufficiently, the cycle can begin again. What was not known at the start of this effort was whether this phenomenon could also produce a directed, pulsed jet. To attempt this, a cylindrical shroud was placed around the tube and jet, to collect the air leaving the tube and direct it out the back of the shroud. Hartmann–Sprenger tubes have been shrouded previously (Brocher and Pinna [20]), but with acoustic horns, with the objective of amplifying the sound. These acoustic horns were closed at the end where the source is located, and increased in area with distance away from the source. The flow from the horn would therefore be diverging, and the velocity at the exit would be reduced in value from that leaving the source. To create a more concentrated flow, a cylindrical shroud was used in the present work. This shrouded tube did produce periodic structures traveling along the extended axis of the device.

The filling of the resonance tube corresponds to a compression wave traveling down the tube, which is reflected at the closed end as a hammer shock. When this hammer shock reaches the open end, starting the emptying phase, a reflected expansion wave is created. This travels down the tube, is also reflected from the closed end, and the filling phase begins when the reflected expansion returns to the open end. Thus the frequency of operation is approximately the quarter wave frequency based on the length of the closed tube [13,20], although it departs from this for tubes whose length is of the order of their diameter [18]. For the shrouded tube it is also dependent on the length of the shroud.

The shrouded tube used at a frequency of 550 Hz is shown in Fig. 1. A Mach 2 axisymmetric nozzle with a 12.7 mm diameter throat was aligned with a resonance tube 152 mm in length, internal diameter 16.8 mm, and external diameter $d_t = 25.4$ mm. This was surrounded by a shroud of internal diameter $D_s = 50.8$ mm. A needle was aligned with the axis of the jet to stimulate oscillations, as demonstrated by Brocher [19]. Use of the needle makes the device relatively insensitive to the distance between nozzle exit and the tube entrance. A supply of air at a pressure of 7.8 atmospheres ensured Mach 2 operation in the nozzle when exhausting directly to the atmosphere. The average mass flow was measured upstream of the nozzle, using an orifice meter, and was $0.205 + 0.001$ kg/s. The flow inside the nozzle, tube and shroud has been calculated by Xia et al. [43]. To generate a frequency of 1100 Hz, a plug was inserted into the resonance tube, effectively shortening it to 76 mm in length. New, longer tubes and shrouds were built for frequencies of 275 and 125 Hz.

B. Measurements

To measure the properties of the periodic structures produced, the rings were sampled with a pair of fast response transducers (Endevco model 8530C-50), each built into the nose of a 9.5-mm-diam hemisphere-cylinder body, as shown in Fig. 2, and separated by a distance of 25.4 mm. The probes were inserted into the flow 76 mm downstream of the jet exit. The signals from the probes were displayed on an oscilloscope, using dc coupling, Fig. 3b. The pair was moved radially to generate a plot of pulse pressure versus radius for the structures, Fig. 3b. Then, by spacing the probes equidistantly from the jet axis, at the radius R_{pmin} at which the probes gave the minimum pressure signals (the minima being sharper than the maxima), but separating the probes axially, a measurement of the axial velocity of the structures could be made. The geometry of the probes relative to the Hartmann–Sprenger tube for the velocity measurements is shown in Fig. 4a, and oscilloscope traces in Fig. 4b. This measurement was repeated for each frequency.

At the 275 Hz frequency, one of the high-frequency pressure probes was also placed at the jet exit to obtain the jet exit velocity as a function of time.

Also, for the 275 Hz frequency only, a digital particle image velocimeter (DPIV) [31], as described by John et al. [44], was used to give a velocity and vorticity map of the structures. For this, the Hartmann–Sprenger tube was mounted inside an acrylic test chamber measuring 1220 mm long by 610 mm wide by 610 mm high. Optical access ports at the top and bottom of the chamber, sealed with borosilicate glass allowed entry and egress of the laser beam. The laser beam was provided by a dualhead pulsed Nd:YAG laser (Continuum Surelite III) generating a pair of 400 mJ pulses at 532 nm per firing. Optics converted the beams into light sheets approximately 300 mm wide and 0.25 mm thick. The light sheets were oriented vertically, passing through the extended axis of the Hartmann–Sprenger tube, with the 300 mm dimension along the axis. Each laser pulse was synchronized with a single 2048 by 2048 pixel cross-correlation camera (Redlake Megaplus ES 4.0), viewing the laser sheet horizontally. The firing of the lasers was controlled by a signal from a time delay generator triggered by a signal from a

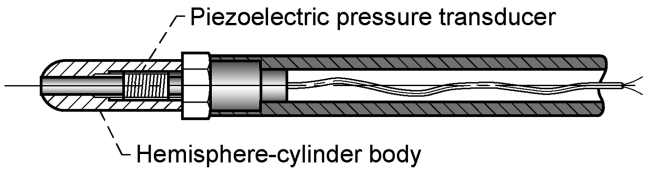

Fig. 2 Schematic drawing of the high-frequency pressure probe.

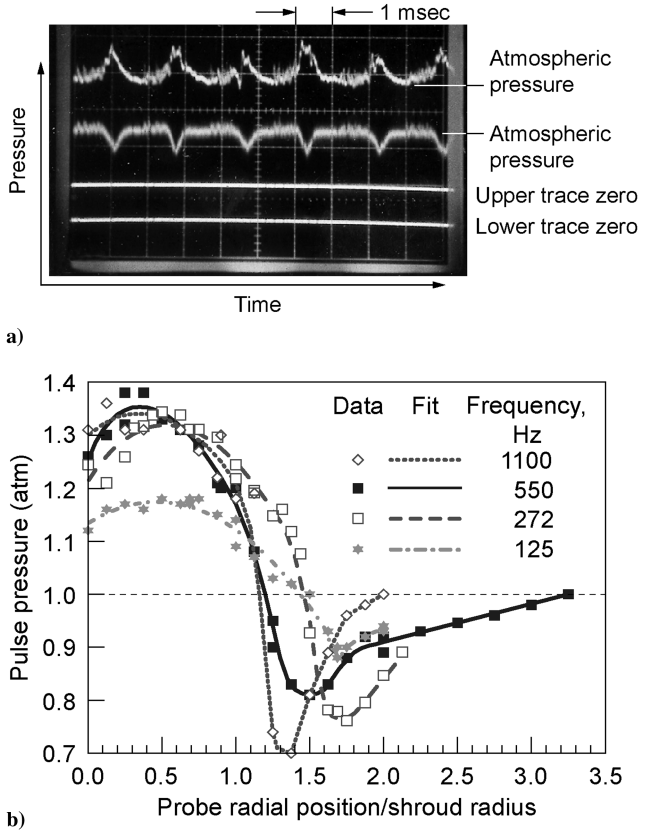

Fig. 3 a) Oscillogram showing pressure probe signals. b) Pressure pulse extrema vs normalized probe position.

pressure transducer mounted in the shroud wall, close to the exit of the shroud. By varying the delay time, data could be taken at different times after the flow leading edge had left the shroud, corresponding to different positions of a single structure along the axis. At any position 200 dual images were taken, and the results were averaged. The acquired DPIV data were processed with PIVROC, a DPIV data processing software package developed in-house at NASA Glenn Research Center [45]. The data were cross-correlation processed in a multipass mode using window offsets in the second pass. The initial pass interrogation window size was 64×64 pixels with 50% overlap, followed by a second pass using 32×32 pixel interrogation windows, again with 50% overlap. The processed data grid spatial resolution was 2.2 mm. The maximum displacements measured were 4 pixels, yielding an full-scale error of 2.5%. At each phase step in the Hartmann–Sprenger tube cycle, 200 individual velocity vector maps were ensemble averaged, yielding a final measurement error of less than 1% of full scale.

The purpose of the test chamber was to contain the seeding material, which was blown in by an air carrier at the upstream end of the chamber, and exited at a hole at the downstream end of the chamber connected to a pipe which deposited the seed outside the laboratory. The flow from the Hartmann–Sprenger tube was also directed into this pipe. Additional seed was injected into the Hartmann–Sprenger tube shroud at the upstream end. The seed consisted of 0.7 μm alumina particles, having a response time of about 0.1 ms [46].

III. Experimental Results

A. Pressure Probing

Signals from the high-frequency pressure probes sampling the structures at an axial distance (usually 76 mm) from the nozzle exit, are shown in the oscillogram in Fig. 3a, taken at a frequency of 550 Hz. Similar to the sketch in Fig. 4b, two probes were used, both aligned with the z-axis, but spaced 25.4 mm apart, with $s = 0$. The probe pair was moved radially to generate the plot in Fig. 3b, in which

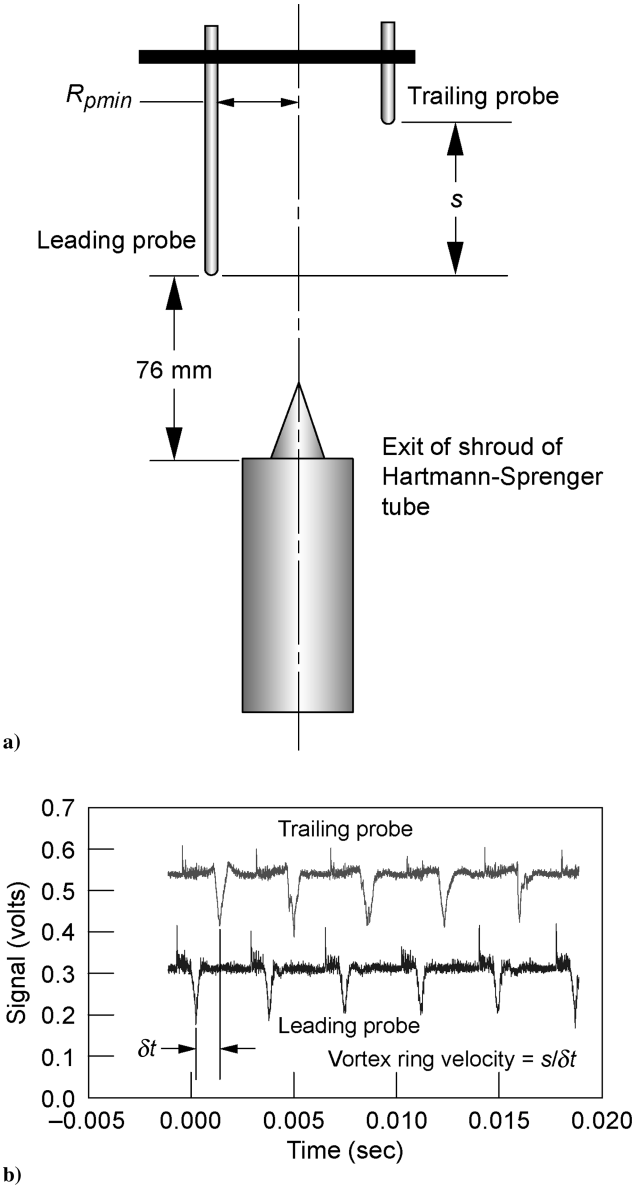

Fig. 4 a) Geometry of the pressure probes for, and b) oscillogram obtained in measuring W.

the upper oscillogram is from the probe closer to the axis of the jet, and exhibits a rise in pressure with time, followed by a decay, returning to atmospheric pressure at about half the period of the pulses. After the signal returned to atmospheric, there appeared to be a high-frequency oscillation on it, lasting until the next pulse. As the probe was moved radially, away from the jet axis, the value of the peak pressure first increased slightly, then decreased to zero at a radial position equal to about 1.2 times the jet radius. At distances greater than this, a pulse was seen which was a decrease in pressure, with a minimum pressure well below atmospheric, as shown by the lower oscillogram in Fig. 3a, which is from the probe further from the axis. The values of the pulse extrema, in atmospheres, are plotted as a function of distance from the jet axis in Fig. 3b. For a frequency of 550 Hz, the absolute outer edge of the disturbance, where there is no longer any signal, is at a radial position of 3.2 times the jet radius, i.e., 81 mm. These measurements were repeated at each frequency used. Because low pressures are expected in the core of a vortex ring, periodic pulses of low pressure are consistent with the flow being a series of vortex rings, though not definite proof.

The positive signals are generated when the probe is acting as a pitot probe, with flow directed towards the transducer. The negative signals are partly generated when the probe is in the low pressure cores, such that the flow is in the opposite direction, and the probe is

Table 1 Measured vortex ring velocity, W

	$f = 1100$ Hz	$f = 550$ Hz	$f = 275$ Hz	$f = 125$ Hz
W from pitot probes, m/s	73 ± 8	77 ± 13	90 ± 12	77 ± 12
W from DPIV	——	——	79 ± 3	——

acting more like a static pressure probe. This will become more obvious in the following sections.

As stated, to measure the axial velocity of the structures, W, the probes were separated axially by a distance of 100 mm, and were each at a radial distance from the axis such that they were sampling the pressure minima; see Fig. 4. Velocities derived from these signals are given in Table 1. Each velocity is an average of at least 16 readings. Some variation in velocity with probe axial separation, and with position of the leading probe relative to the nozzle exit, was observed, but was less than the experimental error.

B. Digital Particle Image Velocimetry

Digital particle image velocimetry was used to measure velocities within the vortex ring, for a frequency of 275 Hz only. Digital particle image velocimetry provides axial and radial velocity, and vorticity information within the entire flowfield. As shown next, these images confirmed that the structures are indeed vortex rings. To evaluate the data, the flowfield is divided into a grid with spacings $\delta r = 2.26$ mm radially by $\delta z = 2.26$ mm axially, with data values at each node. The radial extent of the grid is 75.9 mm upwards, and 57.3 mm downwards, and the axial extent is 232 mm measured from the outer shroud edge. Twenty-two time delays were used to give different positions of the vortex ring plane, which is defined as the plane, normal to the axis, which contains the vortex core centers. The vortex ring plane was found by searching within the data, at any one vortex ring position, for the radial and axial point at which the absolute value of vorticity was a maximum, and the radial velocity was zero. There were two points, one radially above the z-axis and one below. The average value of z for the two points was taken as the vortex position, and the average value of r as the vortex radius R. Values of z for each position of the vortex ring plane are plotted against time (from the time delay generator) in Fig. 5. The data are fitted very well with a least-squares straight line, indicating that the velocity is nearly constant. The slope of the line is the vortex ring velocity, W, with a value of 79 ± 2.6 ms. The largest error in this measurement is the grid spacing, and is indicated by the vertical size of the square symbols. Clearly, positions are not known to any better precision than this; however, the resulting velocity is quite well defined.

At any position of the vortex ring, the axial velocity and vorticity along the vortex ring axis can be plotted. This is done in Fig. 6 for the ring position of $z/D = 1.94$. It can be seen that the axial velocity is symmetrical about the z-axis, and the vorticity is antisymmetrical, the axial velocity being consistent with the distribution of velocity in a vortex ring as described by Maxworthy [29]. The vorticity distribution is qualitatively similar to distributions in Fig. 14 of Gharib et al. [38], except that, unlike that figure, here there is a region for $r < r_0$ for which the vorticity is opposite in sign from that for $r > r_0$. The region with $r < r_0$ presumably contains vorticity shed at the inner edge of the annulus. Thus it does indeed appear that the flow consists of a series of vortex rings. There are maxima and minima in the axial velocity distribution: the maxima occur at $r = R - a$ (assuming that the core is reasonably circular), and the minima are at $r = R + a$ [36,47,48]. Thus four values of a can be derived from Fig. 6. In addition, as pointed out by Maxworthy [29], values of a can be derived from the values of z at the maximum and minimum values of radial velocity at $r = R$. In Fig. 7, the values of R, the average of the values of a, and the corresponding values of ε are plotted for each normalized ring position. The lines are linear least square fits to the data. It is seen that the core size and radius grow with z/D, but that ε is approximately constant at a value of about 0.6. The outer edges of the cores are not very well defined. This is because the vortex rings are turbulent, as will be demonstrated next. It should be noted that values of a derived from the axial velocity maxima and minima were not noticeably different from those derived from the radial velocity, indicating that the cores are roughly circular. This is at odds with calculations of Norbury [49], who found that at $\varepsilon = 0.6$, the cores are stretched out in the axial direction, with the axial extent of the core being about 1.4 times the radial extent.

By assigning a gray scale value to a range of vorticity, contour plots of vorticity at each value of z/D can be made. Three examples are given in Fig. 8, for $z/D = 0.45$, 1.94, and 4.0. The center of the vortex cores appears white above the horizontal axis, and black below it. The plot at $z/D = 1.94$ is of most interest because this is the location of the ejector entrance that gives the maximum thrust augmentation [5]. From Fig. 6, for $z/D = 1.94$, $R = 33.3$ mm, $a = 20$ mm, and hence $\varepsilon = 0.6$. The minimum signals from the pressure probes do not occur at the core center. In fact the pressure minimum is at a radius of 43 mm, which is the radius at which the DPIV data show that the velocity is zero, from Fig. 6. This radius is $R + 0.5a$. For greater radii, the velocity over the probes is negative,

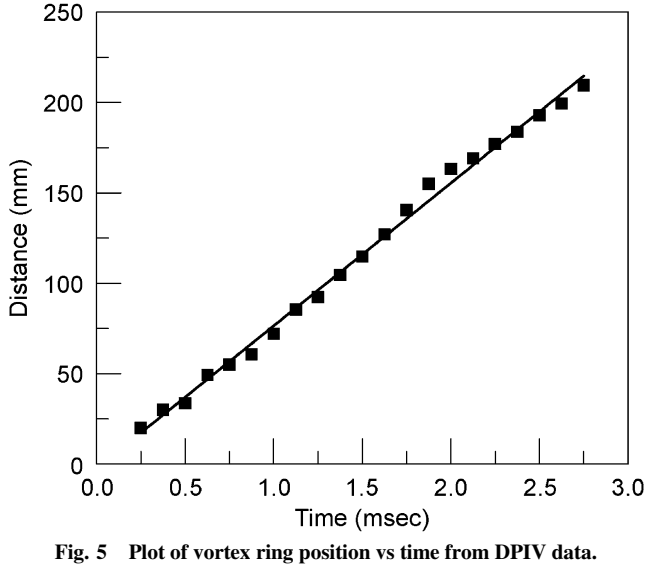

Fig. 5 Plot of vortex ring position vs time from DPIV data.

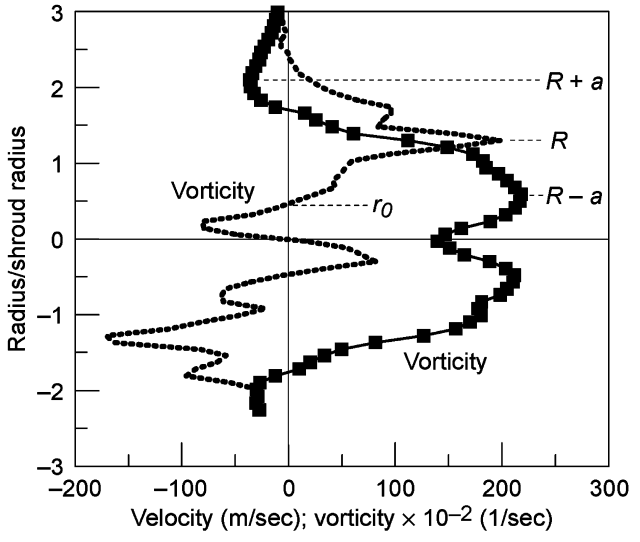

Fig. 6 Velocities (■) and vorticity divided by 100 on the r-axis through the vortex ring.

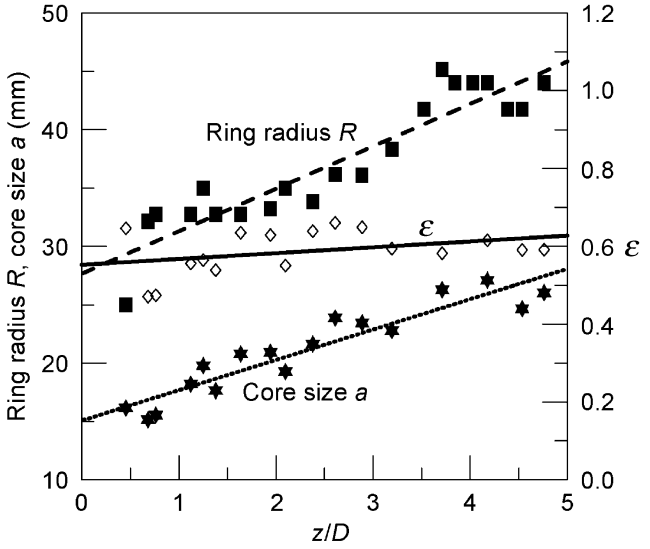

Fig. 7 Vortex ring radius R, core size a, and ε vs z/D.

so they are not then acting as total pressure probes. The plot at $z/D = 4.0$ is interesting in that it shows that the negative vorticity in the region $r < r_0$ has either decayed, or been completely absorbed into the vortex ring.

The DPIV data provide a map of vorticity over the entire field of view. In principle, the circulation in the vortex ring can be determined from the vorticity by performing the integral

$$K_{\text{ring}} = \iint \omega \, \mathrm{d}r \, \mathrm{d}z \tag{1}$$

over a region around the core, along whose boundaries the vorticity is zero. Such a region is difficult to find. It has been shown by Gharib et al. [38] that for vortex rings generated by a pulse with a value of L/D greater than a limiting value, which is called the formation number, the flow is a vortex ring followed by a trailing jet. As will be shown later, the pulse at 275 Hz does have a value of L/D greater than F, and the trailing jet can be seen in Fig. 8. The trailing jet also contains vorticity, and in Fig. 8, it not easy to separate the trailing jet from the vortex ring. For the ring position $z/D = 1.94$, the region shown as a solid line around the vortex core in Fig. 8b seems to include the vortex ring positive vorticity, while excluding that from the trailing jet. Replacing the integral with a summation, the circulation for this region is

$$K^{+}_{\text{ring}} = \sum_{r_0}^{76.5} \left(\sum \omega \delta z \right) \delta r \tag{2}$$

i.e., at each value of r within this region, the product of $\omega \, \delta z$ is summed for all values of vorticity between the limits of z, and the resulting summations multiplied by δr are summed from r_0 to the maximum value of r. Similarly, the negative circulation from the axis to $r = r_0$, enclosed within the dashed lines in Fig. 8b, which is presumably circulation shed from the inner edge of the annulus, can be calculated as

$$K^{-}_{\text{ring}} = \sum_{0}^{r_0} \left(\sum \omega \delta z \right) \delta r \tag{3}$$

The result is $K^{+}_{\text{ring}} = 12.2$ m^2/s, and $K^{-}_{\text{ring}} = -3$ m^2/s, for a net circulation of 9.2 m^2/s. Clearly the negative vorticity shed at the inner diameter is insufficient to cancel that shed at the outer diameter. The lower boundary drawn in Fig. 8b is actually not r_0, but the lowest line having only positive vorticity. If the positive circulation below that is included, it adds a further 0.2 to K^{+}_{ring}. Similarly, the circulation in the trailing jet, K_{tj}, can be evaluated, with the result that $K_{\text{tj}} = 14.9$ m^2/s.

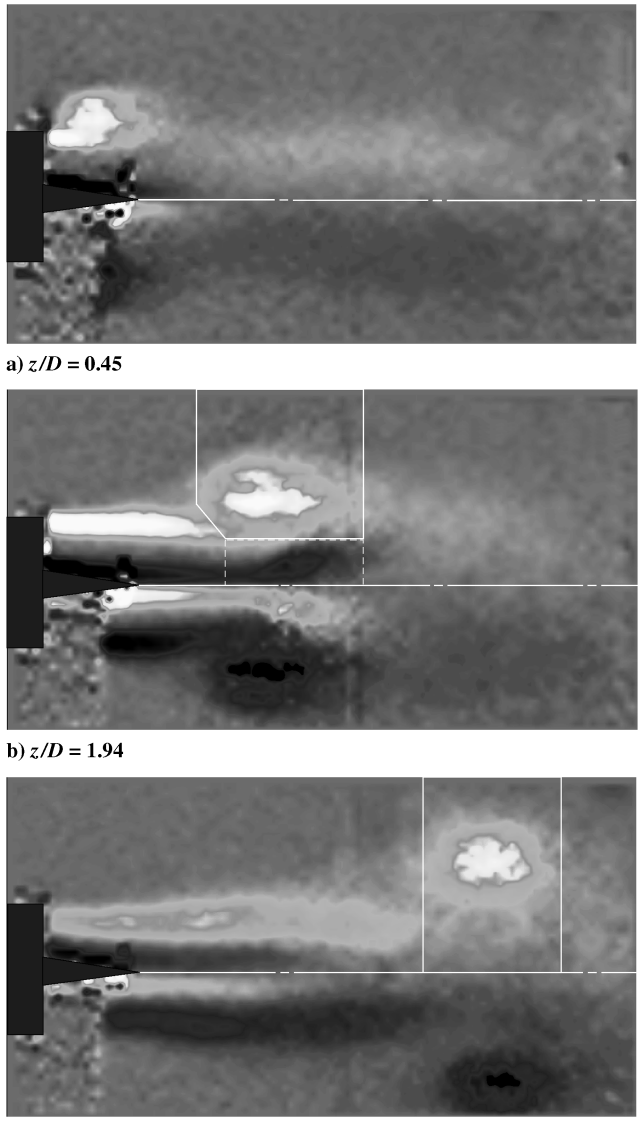

a) z/D = 0.45

b) z/D = 1.94

c) z/D = 4

Fig. 8 Vorticity maps of the flowfield at different positions of the vortex ring.

By the time that the vortex ring has reached $z/D = 4$, the negative circulation has vanished, and thus $r_0 = 0$. From Fig. 8c, the ring circulation is contained within the region $z/D = 4 \pm 0.68$, or $z =$ 147 to 207 mm, indicated by the vertical lines, which excludes any circulation from the trailing jet. Thus the summation

$$K_{\text{ring}} = \sum_{0}^{76.5} \left(\sum_{147}^{207} \omega \delta z \right) \delta r \tag{4}$$

will give the ring circulation at $z/D = 4$. The result is $K_{\text{ring}} = 12.5$ m^2/s. This is very close to the value of K^{+}_{ring} for $z/D = 1.94$, indicating that the negative vorticity close to the centerline in Fig. 8b has diffused across the centerline and cancelled out, without affecting the vortex ring circulation.

C. Jet exit velocity

By placing one of the high-frequency pressure probes used to sample the vortex ring exactly in the exit plane of the jet, a signal is obtained which can be related to the jet exit velocity. This was done at a frequency of 275 Hz only. The resulting velocity program is plotted in Fig. 9. The flow starts with a weak shock wave (Mach number = 1.25), and, after an initial spike, is approximately constant for awhile before falling off. The product of an average flow

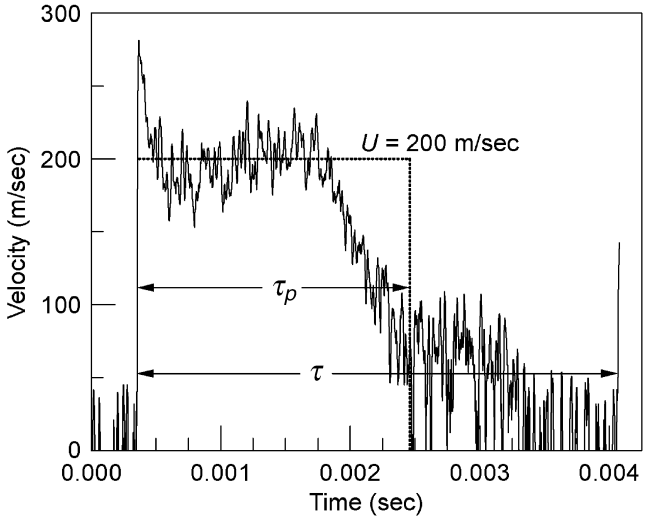

Fig. 9 Velocity program at the Hartmann–Sprenger tube shroud exit.

exit velocity times the equivalent square wave pulse length can be derived from the mass flow, namely,

$$\dot{m}_{\text{jet}} = \rho U(\pi/4)D^2(\tau_p/\tau) \tag{5}$$

The average velocity during the approximately constant part of the velocity program is 200 m/s. Because this is the portion of the pulse during which the vortex ring is formed, this will be taken as the equivalent square wave velocity U. With $U = 200$ m/s, τ_p/τ has a value of 0.57 from Eq. (5). This is not unreasonable, as the Hartmann–Sprenger tube cycle consists of filling the resonance tube for roughly half the cycle, and emptying it during the remainder of the cycle. The equivalent square wave is shown in Fig. 9. The value $U = 200$ m/s will be used for normalizing vortex ring propagation velocity data. In deriving L/D vs ε for a jet with velocity that is not constant with time using slug theory, the integrals $\int u(t)\,dt$, $\int u(t)^2\,dt$, and $\int u(t)^3\,dt$ are required (see Appendix). These can be obtained from the data of Fig. 9.

IV. Assessment of the Experimental Accuracy

To determine the size of the vortex rings, the pressure probes and DPIV images were used. A major inaccuracy in the probe measurement was setting the probes at the claimed location. The system used was not very sophisticated, and it is estimated that radial measurements could be in error by 0.5 mm. This is true of the position of the probe as well as the centerline from which it was measured, for a total possible error of 1 mm. In addition, the finite size of the pressure sensor (3 mm) adds imprecision to the location of the pressure minimum. Together these result in an uncertainty in r/D of ± 0.07, as indicated in Fig. 10. For the vortex ring velocity measurements, the pressure probes were staggered, and the travel time between the probes was measured. The distance between probes was 100 mm, which could be measured reasonably accurately. The travel time proved somewhat variable, however. Consequently, at any frequency, at least 16 different readings of the time, as read from an oscilloscope, were taken, to provide an average, standard deviation, and 95% certainty estimate. The error bars in Fig. 10 correspond to the 95% confidence interval. In the case of the DPIV measurements of vortex ring velocity, the vortex ring position was determined as the average of 200 images at each of 21 different time steps, as shown in Fig. 5. A linear least-squares fit to the data provided the average velocity, plus the standard deviation in velocity, and the 95% confidence interval, which is plotted in Fig. 11.

The average velocity assigned to the flow at the exit of the nozzle, U, was derived from the instantaneous velocities given in Fig. 9. What was actually measured was the pitot pressure as a function of time. This was translated to velocity assuming quasi-steady flow relations, and assuming that the flow stagnation temperature was

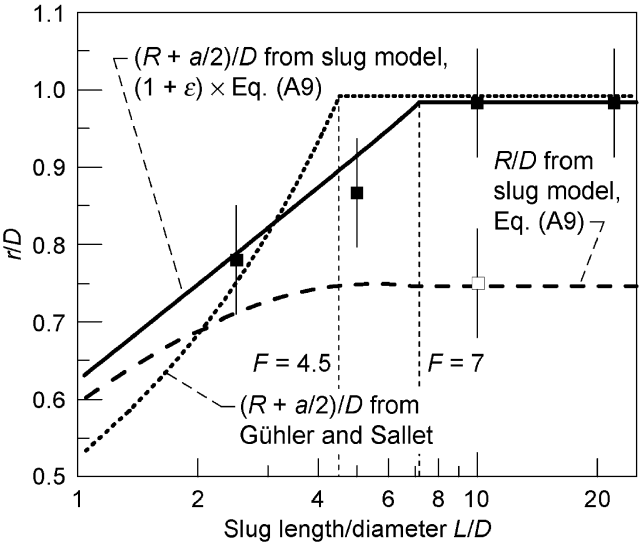

Fig. 10 $R_{p\,\min}/D$ pressure probe data (■), DPIV measurement of R/D (□), and calculated values.

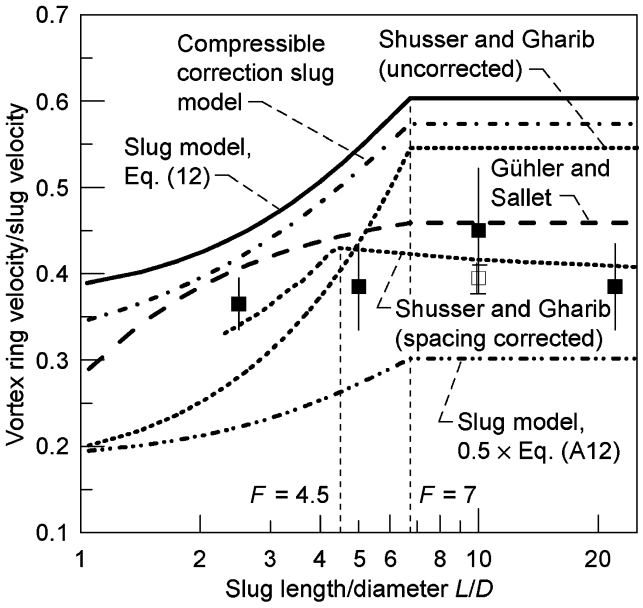

Fig. 11 Normalized vortex ring velocity vs L/D: calculations, pressure probe data (■), and DPIV data (□).

room temperature, i.e., 290 K. However, the Hartmann–Sprenger tube cycle involves a hammer shock inside the resonance tube to bring the Mach 2 flow to rest. This will increase the entropy of the air, bringing it to a calculated stagnation temperature of 386 K. With this stagnation temperature, the pressure rise that gives a velocity of 200 m/s if the stagnation temperature were room temperature, generates a velocity of 230 m/s. Unfortunately, no measurement of temperature of the jet was made. Consequently, the value of U is not well established, but is expected to be around 200–230 m/s.

V. Comparison Between the Slug Model and Experimental Results

The experiments were performed at four different frequencies. Because the throat of the Mach 2 nozzle was choked, the mass flow was constant at all frequencies, and the mass per pulse m_p is given by

$$m_p = \dot{m}_{\text{jet}}/f \tag{6}$$

But m_p is also given by the product of pulse volume and density

Table 2 L/D and ε for each frequency used

Frequency, Hz	1100	550	275	125
L/D	2.5 ± 0.02	5 ± 0.04	10 ± 0.1	22 ± 0.2
ε	0.22 ± 0.001	0.44 ± 0.004	0.6 ± 0.007	0.6 ± 0.007

$$m_p = \rho\pi(D_s^2 - d_t^2)L/4 \tag{7}$$

from which it is seen that L, and hence L/D, is inversely proportional to frequency. In referring to the slug flow model (Appendix A), it is clear that the appropriate effective diameter appearing in the calculation of L/D [Eqs. (A2) and (A3)] is twice the square root of the flow area divided by π, so that for the Hartmann–Sprenger tube it is $D = \sqrt{(D_s^2 - d_t^2)}$.

In Table 2, the values of L/D for each frequency used are given together with values of ε from Eq. (A4) together with Eq. (A15) for the two higher frequencies. For the lower frequencies, the vortex probing showed that the pressure minima were at the same radius for both frequencies. Calculations using the slug model (see the Appendix) show that $(R + a/2)/D$ increases monotonically as L/D increases (although R/D may not), apparently at odds with the preceding result. However, Gharib et al. [38] showed that above the formation number, the circulation of the vortex ring remains constant as L/D increases, with the remaining circulation going into a trailing jet, and that the vortex ring size remains approximately constant. Thus it was concluded that the two lower frequencies have L/D above the formation number, and that, because the same apparatus produced both sets of vortex rings, with the only change being the value of L/D, ε is the same for both, and equal to the value measured from the DPIV data, namely, 0.6. It is clear from the DPIV data in Fig. 8b that there is a trailing jet for $L/D = 10$, so that this case is definitely above the formation number. In the case of Gharib et al., the formation number was 4. If this were the case for the present experiments, the vortex rings for 550, 275, and 125 Hz, which all have L/D greater than 4, should be the same size, and so the pressure minima should be at the same radius. In fact the 550 Hz pressure minima are at a smaller radius than are those at 275 and 125 Hz. This indicates that the formation number appears to be at a higher value of L/D than 4. As mentioned in the introduction, slug theory (outlined in the Appendix) has been used to relate vortex ring properties to properties of the flow generating the vortex rings. In using slug theory, it is important to recognize that the circulation in the vortex ring may differ from that nominally assigned to the slug, namely, $UL/2$, i.e., Γ may differ from unity. At small values of L/D, it is found that $\Gamma > 1$, but at high values of L/D, $\Gamma < 1$ [37]. The value of Γ affects the calculated vortex ring and core radii, and the vortex ring velocity. In the Appendix, a relationship for Γ as a function of L/D is described which gives agreement between calculated values of R/D and measured values of R/D obtained by Liess and Didden [28], and so seems to be a reasonable choice. This is Eq. (A15). Using Γ from Eq. (A15), and also Eq. (A4), ε can be calculated, and the value of ε observed, i.e., 0.6, is calculated to be at an L/D of 7. This then appears to be the formation number for these vortex rings.

Another rough measure of the formation number is the value of $(L/D)K_{\text{ring}}/(K_{\text{tj}} + K_{\text{ring}})$. Using values from the DPIV data for $z/D = 1.94$, this equates to 4.5, close to the value found by Gharib et al. [38]. However, Krueger and Gharib [41] point out that for a train of pulses, the trailing jet from a preceding pulse tends to remain near the nozzle, and affects the formation of the pulse. Thus the value of K_{tj} measured from Fig. 8b may not be representative of a single pulse.

From the velocity program of the pulse, given in Fig. 9, the value of $K_{\text{slug}} = \int u(t)^2\,\mathrm{d}t/2$ can be calculated, and is equal to 35.7 m^2/s. If $F = 4.5$, using Eq. (A15) to calculate Γ for $F = 4.5$ leads to $K_{\text{ring}} = \Gamma\, K_{\text{slug}}F/(L/D)$, with a value of 13.2 m^2/s. On the other hand, if F = 7, the same calculation gives $K_{\text{ring}} = 19.1$ m^2/s. The value of K_{ring} for $F = 4.5$ is clearly much closer to the value of 12–12.5 obtained from the DPIV measurements than is the value for $F = 7.0$. Thus there is contradictory evidence for whether $F = 4.5$ or 7. The values of $(L/D)K_{\text{ring}}/(K_{\text{tj}} + K_{\text{ring}})$ and K_{ring} point to $F = 4.5$, whereas the values of R_{pmin}/D suggest $F = 7$.

The DPIV data showed the vortex ring radius R to be 33 mm, and $\varepsilon = 0.6$. With a formation number of 7, the ratio Γ is found to be 0.766 from Eq. (A15), and $I(\varepsilon) = 3.888$ for $\varepsilon = 0.6$ from Table 4. Inserting these values into Eq. (A9a) gives $R = 32$ mm with the diameter equal to D, in good agreement with the DPIV value. If instead, D_s is used, R is calculated to be 37 mm. Thus, even though the shear layer is generated at D_s, D is the appropriate diameter for modeling the vortex ring radius. The DPIV value of $R/D = 0.75$ is plotted in Fig. 10, together with the calculated value of R/D using the slug model with Γ given by Eq. (A15). The measurement is in good agreement with the calculation. Note that the calculated R/D changes very little between $L/D = 4.5$ and $L/D = 7$, so this measurement is consistent with $F = 4.5$ and $F = 7$.

The probe measurements in Fig. 3b show that the pulse minima are at a value of $R_{\text{pmin}}/R_s = 1.7$ for the 275 and 125 Hz rings, where R_s is the shroud radius. The DPIV data in Fig. 5 indicate that this is the radius at which the velocity is zero, and is equal to $R + 0.5a$. Assuming then that the probe minima are at a radius of $R + 0.5a$, values of $(R + a/2)/D$ can be calculated and plotted against L/D for comparison with the measured values of R_{pmin}/D. Calculated values of $(R + a/2)/D$ from the slug model (Appendix), assuming a

Table 3 Velocity-time relationship for turbulent vortex rings

Reference	Medium	Velocity-time relation	z/D range
Wiegand and Gharib [50]	Water	$W = 0.10$, $W = 14.88 - 2.16t$	0–9.5, 9.5–22
Maxworthy (1977) [29]	Water	$W =$ constant	——
Sallet and Widmayer [33]	Air	$W \sim t^{-1/2}$	12–48
Maxworthy (1974) [27]	Water	$W =$ constant	>15
Glezer and Coles [54]	Water	$W \sim t^{-3/4}$	5–50
Johnson [32]	Air	$W \sim t^{-1/3}$	<70

Table 4 Values of the nondimensional vortex ring impulse $I(\varepsilon)$, energy $E(\varepsilon)$, and velocity W/U

ε		0.2	0.4	0.6	0.8
$I(\varepsilon)$	Norbury	3.226	3.422	3.653	3.888
	Fraenkel	3.236	3.519	3.990	4.650
	Fit [Eq. (A7)]	3.229	3.419	3.656	3.888
$E(\varepsilon)$	Norbury	1.00	0.673	0.526	0.437
	Fraenkel	0.997	0.713	0.595	0.553
	Fit [Eq. (A8)]	1.00	0.685	0.527	0.436
W/U	Norbury	0.4363	0.5353	0.6019	0.6522
	Fraenkel	0.4393	0.5188	0.5761	0.6026
	Fit [Eq. (A11)]	0.4381	0.5272	0.6034	0.6516

formation number of $L/D = 7$, and using the values of ε versus L/D calculated from Eqs. (A4b), (A6), and (A8), with Γ from Eq. (A15), are given in Fig. 10, together with the measured values of R_{pmin}/D.

Gühler and Sallet [30] derived a semiempirical equation for R by equating the mass of fluid in the slug to that in the vortex ring, with the result that

$$2R/D = (L/D)^{1/3} \tag{8}$$

which fitted their data well from $L/D = 1$ to 4.3, but overpredicted R above that. In fact, their experimental value of R seems to be constant above $L/D = 4.3$, suggesting that this is their value of formation number. They found that other models for calculating R did not agree with their data; these have not been added to Fig. 10. Values of $(R + a/2)/D$, using R from Eq. (8), and ε from Eqs. (A4b), (A6), and (A8), together with Γ from Eq. (A15) are also plotted in Fig. 10 as a function of L/D. If it is assumed that the formation number is 7, this calculation would produce very large values of R_{pmin}/D at the formation number. Assuming a formation number of 4.5, however, generates approximately the same value of R_{pmin}/D as does the slug model. Thus it would appear that there is little to distinguish between the results of the slug model with $F = 7$, and Eq. (8) using $F = 4.5$. One difference is that the value of R/D calculated from Eq. (8) at $L/D = 4.5$ is 0.83, somewhat larger than the value of $R/D = 0.75$ measured by DPIV. In addition, with a formation number of 4.5, the calculated value of ε is 0.4, whereas with a formation number of 7, the calculated value of ε is 0.6, the value observed using DPIV.

In fact, however, the calculated values of ε cannot really be compared with the experimental values. The experimental values were based on a core radius a derived from vortex ring velocity maxima and minima; the calculated values (Norbury [49]) are defined by the boundary between rotational flow in the core, and irrotational flow exterior to it. Moreover, the vorticity distribution assumed in the calculation by Norbury ($w \sim r$) is not representative of observed vorticity distributions in the vortex core [36,48]. These studies have shown that vorticity extends to core radii greater than the values of a defined by velocity peaks, and that the vorticity distribution is approximately Gaussian, centered on the core center (i.e., $r = R$). However, calculations by Mohseni et al. [40] with a realistic vorticity distribution in the core have shown little difference between their energy, circulation, and mean core radius, and those of Norbury [49].

In Fig. 11, the observed vortex ring velocities divided by U at $z/D = 1.94$ are also plotted against L/D, together with values calculated from the slug model, using Eq. (A12), with Γ given by Eq. (A15), again assuming that the formation number has a value of 7, and that the circulation and velocity will not change with L/D above the formation number. Two curves, calculated from the slug model are given, one for $K_{\text{ring}} = \Gamma\, U\, L/2$, and one for a propagation velocity half of that. The justification for plotting half the calculated ring velocity is that Wiegand and Gharib [50] state that the initial velocity of a turbulent vortex ring is half that of a laminar ring. Other formulae for vortex ring velocity have been given by Gühler and Sallet [30], and Shusser and Gharib [51]. Gühler and Sallet, using Eq. (8) for the vortex ring diameter, find the velocity of the vortex ring to be

$$\begin{aligned} W/U &= (3+\pi)/4\pi - (3+\pi)/[3\pi^2(L/D)] \\ &= 0.49 - 0.21/(L/D) \end{aligned} \tag{9}$$

Shusser and Gharib, based on an energy variational principle, find that the velocity of a thick vortex ring is

$$W = 0.5352\sqrt{\rho K_{\text{ring}}^3/\pi P} \tag{10}$$

Inserting $P = \rho R^2 K_{\text{ring}} I(\varepsilon)$, using Eq. (A9) to relate R to D, and setting $K_{\text{ring}} = \Gamma UL/2$ in Eq. (10) leads to

$$W/U = 0.12\Gamma^{1.5}(L/D) \tag{11}$$

Equations (9) and (11) are also plotted in Fig. 10, again assuming that $F = 7$.

All the preceding relationships for the vortex ring velocity are incompressible results. However, the value of U shows that the jet flow is around Mach 0.5, and compressibility might have an effect. Moore [52] has calculated that a compressible vortex ring will travel more slowly than an equivalent incompressible vortex ring by an amount

$$\Delta W = 5K_{\text{ring}}M^2/48\pi R + O(M^4) \tag{12}$$

in which the vortex Mach number is defined as $M = K_{\text{ring}}/2\pi ac$. This correction has been applied to the slug flow calculation, with the result shown in Fig. 11. It does lead to a reduction in W/U, but not enough to give agreement with the data. Compressibility might also have an effect on the values of R and a, although the magnitude of this effect is not known.

Even though the data show some scatter, it is clear that the velocity calculated from Eq. (A12) with $K_{\text{ring}} = \Gamma UL/2$ with $F = 7$, is considerably greater than the observed values. It might be thought that the high value of W calculated from the slug theory is because the value of Γ used in Eq. (A1) is too high. However, Γ also appears in Eq. (A9), the equation for the vortex ring radius, so that if Γ were reduced, the good agreement between calculated and observed values both of R_{pmin}/D, and R/D, would be diminished.

VI. Comments

The important quantities for characterizing a vortex ring are its radius R, velocity W, and circulation K [27]. In addition, the functional form of the vorticity distribution is needed if P and T are to be determined. This seems to imply that these are fixed quantities once a vortex ring is formed. In fact, they are not, because vortex rings tend to slow down, and grow in size as they propagate [28], as was seen for R and a in Fig. 7. A detailed discussion of this topic for laminar rings is given in [29]. Therefore comparison with slug theory, which only gives a single value for these quantities, poses some difficulty. Close to the nozzle, the radius has been shown to grow rapidly, then decline, and reach a final value asymptotically [25,36]. However, the asymptotical value is reached at $z/D \sim 1$, after which it grows slowly. Thus an initial value for the radius can be defined after about $z/D = 1$. The actual distance for a vortex ring to form completely has been given as $z/D = 2.5$ by Sallet and Widmayer [33]. Measurements at $z/D = 1.94$ are therefore somewhat premature. Indeed, Fig. 8b shows a much more disorganized vortex ring than does Fig. 8c. Nevertheless, $z/D = 1.94$ is of interest because the objective here is to find relations for the properties of the vortex rings and how they vary with the driving jet frequency, at this location, because it is the location for the ejector entrance which gives the maximum thrust augmentation [5]. Comparisons are therefore to be understood to be at, or close to, this location only. The measurements of R_{pmin}/D shown in Fig. 10 indicate that there is good agreement with the present measurements and values of $(R + a/2)/D$ calculated from slug theory using Eq. (A15) (see Appendix for justification of this value of Γ), i.e., assuming that $R_{\text{pmin}} = R + 0.5a$, which was established at the frequency of 275 Hz only. The formula of Gühler and Sallet [30], Eq. (8), which fitted their data well, has a very steep dependence on L/D, but is a fairly good fit to the data if the formation number is set to 4.5. However, from Eq. (A4), this gives a value of $\varepsilon = 0.4$, which is inconsistent with the DPIV measurements. The assumptions made by Gühler and Sallet in deriving their equation for R/D lead to a value of $\varepsilon = 0.29$, independent of L/D, which is also inconsistent with the DPIV data.

It is important to establish whether the flow is laminar or turbulent. Glezer [53] found a boundary for when vortex rings become turbulent; for $L/D > 4$, a vortex ring is turbulent if its Reynolds number, defined as K_{ring}/ν, is greater than 2.5×10^4. Because the minimum value of K_{ring}, for the frequency of 1100 Hz, is about 10 m^2/s, the minimum Reynolds number is 7×10^5, well above the boundary value. Thus the vortex rings under discussion are all

turbulent, as certainly appears to be the case from the vorticity plots in Fig. 8.

There seems to be some question regarding the velocity of turbulent vortex rings. As indicated in Table 3, there are different results for the vortex ring velocity as a function of time. Most of these results are for much larger values of z/D than are under consideration here. Thus the constant initial velocity, for $z/D < 4$ observed here is probably not inconsistent with these results. A particularly interesting case is that of Wiegand and Gharib [50], who found that their vortex ring was initially laminar, with constant velocity, but at about $z/D = 9$, the vortex ring became turbulent, and thereafter exhibited a velocity decay, with considerable vorticity shedding. In the present experiment, the flow has traveled the length of the shroud before exiting, and is probably already turbulent at the exit (the Reynolds number based on the tube length is around 2×10^6). Thus one would expect the vortex ring velocity to decay immediately, but it does not seem to do so, other than the fact that the circulation appears lower than expected. The measured vortex ring velocities shown in Fig. 11 do not agree with values calculated from Eq. (A12) with $F = 7$, but are higher than half these values, so that neither do they conform to the criterion of Wiegand and Gharib [50] that turbulent velocities are half laminar velocities. The formula of Shusser and Gharib [51] does not appear to have the correct dependence on L/D for these values of L/D, which are higher than where it was found applicable. On the other hand, the measured velocities seem to be in reasonable agreement with values calculated from Gühler and Sallet [30], i.e., Eq. (9). Figure 11 has been plotted assuming $F = 7$, but the conclusions are little different if $F = 4.5$. The formula of Gühler and Sallet is still the best fit, although the formula of Shusser and Gharib is now almost identical to it for $L/D > 4.5$, but is too low for $L/D = 2.5$. The slug model calculation with $F = 4.5$ still overpredicts the data.

The value of x, the spacing between the vortex rings in the train, will be smallest at the highest frequency, namely, 1100 Hz, for which it has a value of 66 mm. Consequently x/R is 2.1, which is sufficiently close that, according to Weihs [42], the mutually induced velocity between rings will cause the velocity of each to be higher than for an individual ring. Based on the calculations of Weihs, the velocity will increase by about 24% for $x/R = 2.1$. At 550 Hz, $x/R = 4.5$, and the increase is about 5%. At lower frequencies, the rings are sufficiently separated that this effect is negligible. If this effect were added to the curves, they would tend to flatten out at low L/D. This is shown for the Shusser and Gharib [51] curve in Fig. 11, assuming the value of F is 4.5, consistent with other determinations [38] of F. This curve is in reasonable agreement with the data, even showing a drop in W/U as L/D increases above F, as the increase in velocity due to spacing decreases as the spacing increases, which might also be indicated in the data. Thus when the spacing correction is taken into account, the curve of Shusser and Gharib gives the best agreement with the data. Note that the compressibility correction should also be applied to the Shusser and Gharib curve, so it will be a little lower when this is done.

The vortex ring circulation, K^+_{ring}, derived from the DPIV measurements at $z/D = 1.94$ and 4 are substantially the same, at 12–12.5 m^2/sec, which is consistent with a constant vortex ring velocity, but surprising considering the vortex shedding seen by Wiegand and Gharib [50]. It is also somewhat surprising that the negative vorticity shed from the inner edge of the annulus does not seem to negate the positive ring circulation, but rather simply dissipate, because the positive ring circulation is about the same at $x/D = 1.94$ and $x/D = 4$. The value of K_{ring} calculated from the slug model, i.e., Eq. (A1b) with Γ from Eq. (A15), and assuming $F = 7$, is 23.5 m^2/s, which is higher than the values derived from DPIV. Even with $F = 4.5$, the calculated value of K_{ring} is 15.8 m^2/s, which is still high, but closer to the observed value.

Thus there is no clear-cut conclusive result to what characterizes these vortex rings. When ring spacing is taken into account, the values of vortex ring velocity are consistent with velocity values calculated from Shusser and Gharib, if $F = 4.5$. The value of the ring circulation calculated from the jet velocity program assuming $F = 4.5$ ($K_{\text{ring}} = 13.2$ m^2/s) is close to the values obtained from DPIV (12–12.5 m^2/s). The ratio of $(L/D)K_{\text{ring}}/(K_{\text{tj}} + K_{\text{ring}})$, which is a measure of F, is also 4.5. The slug model, even with a formula for Γ that provides agreement between calculated values of R and measured values obtained by Liess and Didden [28], although it does give agreement between the calculated value of R and the value obtained from DPIV, does not give correct values of circulation, or vortex ring velocity, On the other hand, the slug model, with $F = 7$, does give approximately the value of ε seen by DPIV. The experimentally observed values of R_{pmin}/D increase between $L/D = 5$ and $L/D = 10$, which seems inconsistent with a value of $F = 4.5$, although there is a fairly large uncertainty in the data, so that the apparent increase may not be real. However, it is probably unrealistic to expect the slug model, which is meant to characterize a single, laminar, incompressible pulse, to be applicable to a situation with a train of turbulent, compressible pulses, and the apparent agreement between slug model results and observed R_{pmin}/D data may be fortuitous.

In hindsight, it is unfortunate that DPIV measurements were not made at all frequencies. This might have shed light on the true value of F, and certainly would have given the values of R, ε, and W at each frequency.

VII. Conclusions

A novel device, namely, a shrouded Hartmann–Sprenger tube has been shown to be a source of a continuous train of vortex rings. The vortex ring size and velocity were measured using probes and DPIV, at four values of L/D, and compared with calculated values from slug theory, and from other workers. Although the vortex ring size appeared to be reasonably well predicted by slug theory, velocity was not. After correction for the effect of ring spacing in a train of vortices, the vortex ring velocities were in agreement with a formula by Shusser and Gharib with $F = 4.5$. The vortex ring circulation, as derived from DPIV measurements and calculated from the velocity program, were in rough agreement, and lower than that predicted by slug theory. Although the flow came from an annulus, only the vorticity produced at the outer edge contributed to the vortex ring circulation; the vorticity of opposite sign from the inner edge dissipated by diffusion across the centerline.

The shrouded Hartmann–Sprenger tube produces a fully pulsed jet, and can be made in different lengths to provide a variety of pulse frequencies.

Appendix: Summary of the Slug Model

In the slug model, as shown in Fig. A1, the pulsed jet is assumed to consist of repeated slugs of fluid, each of length L, with constant velocity U, and density ρ, issuing from a tube of diameter D, as would be produced by a piston impulsively started with velocity U and stopping after a stroke L. Initially, the model will be in the usual form, i.e., for a circular jet orifice, not an annulus. Each vortex ring will have a radius R, and a core of "radius" a. Strictly speaking, the core is not a circle, therefore does not have a radius. However, it is

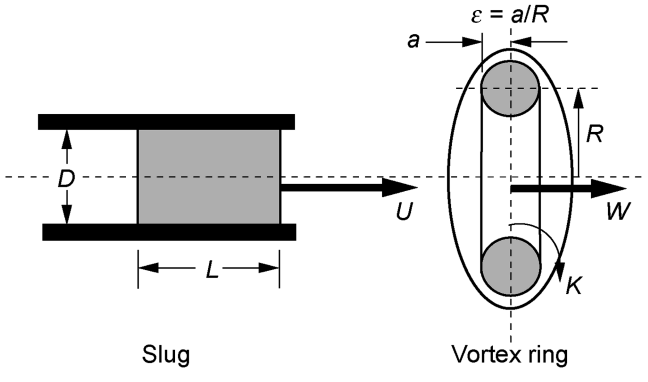

Fig. A1 Schematic diagram of the slug model of vortex ring formation.

approximately circular, and what is meant by a is the square root of the core area divided by π. The value of $\varepsilon = a/R$ is small at small values of L/D, and increases monotonically up to a value of about 0.6 at the formation number.

Given the properties of the jet, Mohseni and Gharib [34] and Linden and Turner [55], have shown that the properties of the vortex, i.e., R, a, and W, are uniquely determined as a function of the value of L/D for the jet. To demonstrate this, they balanced the jet circulation, impulse, and energy with those for the ring, taking the ring values from the work of Norbury [49]. Then with values for the jet in the middle of the following equations, and values for the vortex ring on the right-hand side, the balance equations become

Circulation: for the slug

$$K_{\text{slug}} = UL/2 \tag{A1a}$$

for the vortex ring

$$K_{\text{ring}} = \Gamma K_{\text{slug}} \tag{A1b}$$

Impulse:

$$P = \pi\rho UD^2L/4 = \rho R^2 K_{\text{ring}} I(\varepsilon) \tag{A2}$$

Energy:

$$T = \pi\rho U^2 D^2 L/8 = \rho R K_{\text{ring}}^2 E(\varepsilon) \tag{A3}$$

In these equations, $I(\varepsilon)$ and $E(\varepsilon)$, the dimensionless values of the impulse and energy, are functions of ε only. Following Linden and Turner [55], these equations can be combined to give

$$(L/D)\Gamma^{1.5} = \sqrt{(1/2)\pi(P/\rho R^2 K_{\text{ring}})}/(T/\rho R K_{\text{ring}}^2) \tag{A4a}$$

$$= \sqrt{\pi I(\varepsilon)/2}/E(\varepsilon) \tag{A4b}$$

The right-hand side of this equation, and hence L/D also, is a function of ε only. Norbury [49] solved the equations for a vortex ring numerically, to obtain values of $I(\varepsilon)$ and $E(\varepsilon)$ at a few values of ε. Norbury used a different definition of R than is used here, making it the average of the inner and outer boundaries of the core region containing the vorticity. For values of $\varepsilon \leq 0.6$, the discrepancy is less than about 1%. Also note that $I(\varepsilon)$ and $E(\varepsilon)$ correspond to Norbury's P_N/K_N, and T_N/K_N, respectively, where P_N, K_N, and T_N are Norbury's dimensionless impulse, circulation, and energy. Because the interest here is in small values of ε, at several values of this ratio, it is preferable to have a continuous (in ε) representation. Such a representation was found by Fraenkel [56], who used as a solution a series in ε, valid for small ε. Fraenkel's solutions are

$$I(\varepsilon) = \pi(1 + 3\varepsilon^2/4) \tag{A5}$$

and

$$E(\varepsilon) = 0.5\,\ell_n(8/\varepsilon) - 7/8 + (3\varepsilon^2/16)\,\ell_n(8/\varepsilon) \tag{A6}$$

However, Fraenkel's solution is an asymptotic solution for small ε, which agrees with the Norbury solution as ε tends to zero. Thus for $\varepsilon = 0.2$, the values of $I(\varepsilon)$ and $E(\varepsilon)$ of Fraenkel agree with those of Norbury to within less than 0.3%. However, at $\varepsilon = 0.8$, Fraenkel's values of $I(\varepsilon)$ and $E(\varepsilon)$ exceed Norbury's by 20 and 26%, respectively. To create a better fit for higher values of ε, Fraenkel's expressions were modified to give better agreement with Norbury's values of impulse and energy, by using polynomial fits in ε, giving

$$I(\varepsilon) = \pi(1 + 0.0303\varepsilon + 0.6184\varepsilon^2 - 0.3563\varepsilon^3) \tag{A7}$$

$$E(\varepsilon) = 0.5\,\ell_n(8/\varepsilon) - 0.8594 + 0.098\varepsilon^2\,\ell_n(8/\varepsilon) \tag{A8}$$

Values of $I(\varepsilon)$ and $E(\varepsilon)$ for four values of ε as given by Norbury, Fraenkel, and the series of Eqs. (A7) and (A8) are given in Table 4. As can be seen, the series in Eqs. (A7) and (A8) are good fits to the Norbury values, for ε between 0.2 and 0.8, with the biggest discrepancy being 2% in $E(\varepsilon)$ at $\varepsilon = 0.4$. Values of ε larger than 0.8 will not be needed.

In Fig. A2a, L/D is plotted against ε as a solid line, using Eqs. (A7) and (A8) in Eq. (A4b), with $\Gamma = 1$, as assumed by Linden and Turner. Also, results from Linden and Turner are shown as star-shaped points, for $\varepsilon = 0.2, 0.4$, and 0.6. The agreement is quite good, even for $\varepsilon = 0.6$. The limiting value of $L/D = 4$ is found at a value of $\varepsilon = 0.55$, so higher values of ε than this should not be needed if $F = 4$. The curve of L/D vs ε is in excellent agreement with curves shown in Fig. 1 of Mohseni and Gharib [34] as their Eq. (12), and Fig. 3 of Linden and Turner [55]. This agreement merely shows that Eqs. (A7) and (A8) are good fits to the Norbury data, and does not imply that the model is correct.

The size of the vortex ring is found by combining Eqs. (A1) and (A2) leading to an equation for R/D in terms of $I(\varepsilon)$ and hence, through Eq. (A4b), L/D.

$$R/D = 1/\sqrt{2\Gamma I(\varepsilon)/\pi} \tag{A9a}$$

$$= 1/\sqrt{2\Gamma(1 + 0.0303\varepsilon + 0.6184\varepsilon^2 - 0.3563\varepsilon^3)} \tag{A9b}$$

Substituting Eq. (A5) into Eq. (A9a), and setting $\Gamma = 1$, gives Eq. (21) of Shusser and Gharib [51].

Fraenkel also has an equation for the vortex ring velocity, W, namely,

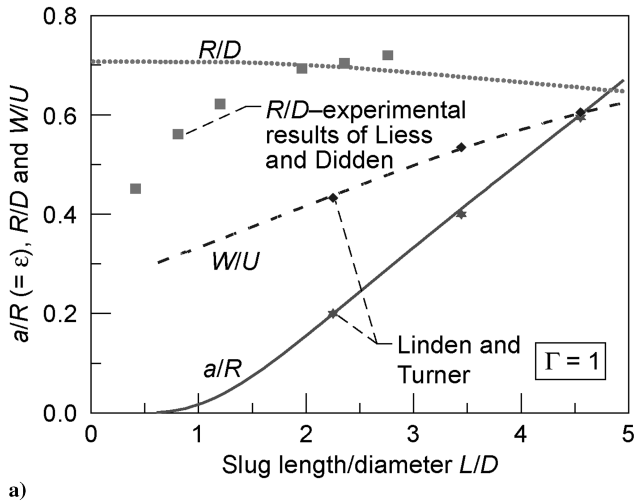

a)

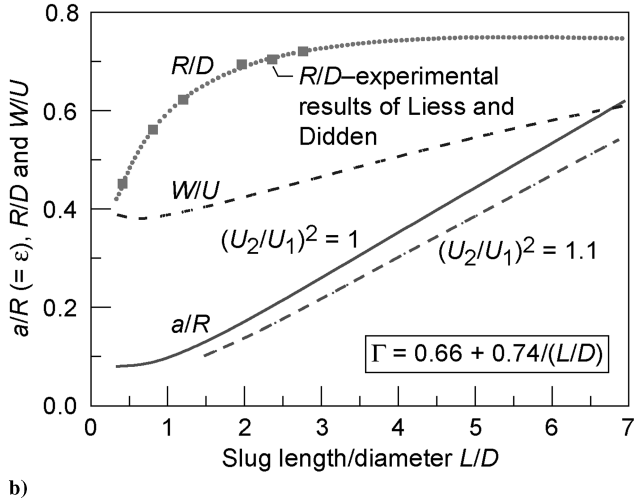

b)

Fig. A2 Slug model calculations of ε, R/D, and W/U with a) $\Gamma = 1$, b) $\Gamma = 0.66 + 0.74/(L/D)$.

$$W = (K_{\text{ring}}/4\pi R)[\ell_n(8/\varepsilon) - 1/4 - \varepsilon^2\{(3/8)\,\ell_n(8/\varepsilon) - 15/32\}] \tag{A10}$$

In the limit as ε tends to 0, this agrees with the equation given by Lamb [57] for small core radius. Again this can be modified to agree with the calculated results of Norbury better, for values of ε up to 0.8, by using the fit:

$$W = (K_{\text{ring}}/4\pi R)[\ell_n(8/\varepsilon) - 1/4 - 0.85\varepsilon^2\{(3/8)\,\ell_n(8/\varepsilon) - 15/32\}] \tag{A11}$$

Using Eqs. (A1) and (A9) in Eq. (A11), the ring velocity divided by the slug velocity is seen to be a function of L/D and ε only,

$$W/U = \Gamma^{1.5}(L/D)\sqrt{2(1 + 0.0303\varepsilon + 0.6184\varepsilon^2 - 0.3563\varepsilon^3)} \cdot [\ell_n(8/\varepsilon) - 1/4 - 0.85\varepsilon^2\{(3/8)\,\ell_n(8/\varepsilon) - 15/32\}]/8\pi \tag{A12}$$

and hence can be expressed in terms of L/D. The values of W/U from Norbury, Fraenkel, and Eq. (A12) are also given in Table 4, again showing good agreement between the Norbury values and the modified fits. R/D from Eq. (9) (dashed line) and W/U from Eq. (12) (dotted line), again for $\Gamma = 1$, are plotted against L/D in Fig. A2a. W/U agrees well with results from Linden and Turner (the diamond-shaped points). However, the calculated values of R/D do not agree with experimental values of R/D from Liess and Didden [28] (the square points) in their dependence on L/D. The calculated values decrease with increasing L/D, whereas the experimental values increase.

Shariff and Leonard [37] have plotted ring circulation divided by slug circulation, i.e., Γ, against L/D, using data from Didden [25], and from Maxworthy [26], and find that this ratio is not unity, and decreases with increasing L/D. They quote two expressions for Γ, an experimental fit by Didden, namely,

$$\Gamma = 1.14 + 0.32/(L/D) \tag{A13}$$

and a theoretical calculation by Pullin [58],

$$\Gamma = 1.41/(L/D)^{2/3} \tag{A14}$$

but neither fits all the data. Both are close at $L/D = 1$, with $\Gamma = 1.4$, which does give the experimental value of R/D found by Liess and Didden. Instead, by finding a value of Γ that also fits the Liess and Didden value of R/D at $L/D = 2.5$, the constants in the following expression were found:

$$\Gamma = K_{\text{ring}}/K_{\text{slug}} = 0.66 + 0.74/(L/D) \tag{A15}$$

This agrees with the two expressions quoted by Shariff and Leonard at $L/D = 1$, and falls between them at $L/D = 2.5$, so it does not seem unreasonable. Admittedly, Shariff and Leonard point out that the reason for the discrepancy between the two expressions may be due to a Reynolds number dependence. This will be ignored here in the interests of simplicity. Using Γ from Eq. (A15), ε, R/D, and W/U were calculated as functions of L/D, and are plotted in Fig. A2b. Now there is excellent agreement between the calculated values of R/D and the experimental values of Liess and Didden [28]. Note that Eq. (A13), used by Didden [25], and subsequently by Wiegand and Gharib [36], which gave good agreement with Didden's data at low values of L/D, is inconsistent with Maxworthy's data [26], and the calculations by Pullin [58], both of which find that at large L/D, $\Gamma < 1$. Obviously Eq. (A13) cannot give this result. On the other hand, Glezer and Coles [54] found that for their turbulent vortex rings, Γ had a value of 1.29 at an L/D of 3.4, so there does not appear to be a universal answer.

It was implicitly assumed that U was a constant independent of time. This is rarely true in practice. If the actual velocity program from the source is represented by $u(t)$ then it follows that $L = \int u(t)\,\mathrm{d}t$, and the jet circulation, impulse, and energy are

$$K_{\text{slug}} = \int u(t)^2\,\mathrm{d}t/2 = U_1 L/2 \tag{A16}$$

$$P = \pi\rho D^2 L/4\left(\int u(t)^2\,\mathrm{d}t \Big/ \int u(t)\,\mathrm{d}t\right) = \pi\rho D^2 L U_1/4 \tag{A17}$$

$$T = \pi\rho D^2 L/8\left(\int u(t)^3\,\mathrm{d}t \Big/ \int u(t)\,\mathrm{d}t\right) = \pi\rho D^2 L U_2^2/8 \tag{A18}$$

where the integrals inside the parentheses define U_1 and U_2, and are taken over one pulse. The right-hand side of Eq. (A4) is now multiplied by $(U_2/U_1)^2$. The effect on the curve of ε versus L/D of having a time-dependent flow is shown in Fig. A2b, for a case with $(U_2/U_1)^2 = 1.1$, corresponding to the velocity program given in Fig. 9.

In summary, given the slug velocity, including its temporal distribution, length and diameter, the vortex ring circulation, radius, and core radius, and hence velocity, can all be determined in principle from slug theory, provided an appropriate value of Γ as a function of L/D is available. However, the results do not always agree well with experiment. Glezer [52] comments that whereas the slug model is unable to predict accurately the magnitude of the circulation, it is useful in predicting relative circulations produced by the same generator. Krueger [59] has shown that the slug model underpredicts the circulation for rapidly initiated jets as it neglects a source term determined by overpressure at the jet centerline during vortex ring formation. It would be useful to know how compressibility and turbulence affect the production of circulation, and vortex ring properties.

Acknowledgments

The assistance of many people in accomplishing this work is gratefully recognized, in particular Wentworth John, for the DPIV studies, and Robert Pastel and Kevin Dougherty for assistance with the experiments. Support from the CVCEE project, directed by Leo A. Burkardt, is also acknowledged with gratitude. Special thanks go to the reviewers, whose conscientious efforts and helpful suggestions significantly improved this paper.

References

[1] Kailasanath, K., "Recent Developments in the Research on Pulsed Detonation Engines," *AIAA Journal*, Vol. 41, No. 2, 2003, pp. 145–159.

[2] Shehadeh, R., Saretto, S., Lee, S.-Y., Pal, S., and Santoro, R. J., "Thrust Augmentation Experiments for a Pulse Detonation Driven Ejector," AIAA Paper 2004-3398, July 2004.

[3] Allgood, D., Gutmark, E., Hoke, J., Bradley, R., and Schauer, F., "Performance Measurements of Pulse Detonation Engine Ejectors," AIAA Paper 2005-223, Jan. 2005.

[4] Rasheed, A., Tangirala, V., Pinard, P. F., and Dean, A. J., "Experimental and Numerical Investigations of Ejectors for PDE Applications," AIAA Paper 2003-4971, July 2003.

[5] Wilson, J., and Paxson, D. E., "Unsteady Ejector Performance: An Experimental Investigation Using a Resonance Tube Driver," AIAA Paper 2002-3632, July 2002.

[6] Paxson, D. E., Wilson, J., and Dougherty, K. T., "Unsteady Ejector Performance: An Experimental Investigation Using a Pulsejet Driver," AIAA Paper 2002-3915, July 2002.

[7] Lockwood, R. M., "Interim Summary Report on Investigation of the Process of Energy Transfer from an Intermittent Jet to Secondary Fluid in an Ejector-Type Thrust Augmentation," Hiller Aircraft Report No. ARD-286, March 1961.

[8] Didelle, H., "L'augmentation de poussée des trompes à jets pulsants ou battants," Doctoral Thesis (in French), L'Université Scientifique et Médicale et l'Institut National Polytechnique de Grenoble, Grenoble, France, March 1976.

[9] Choutapalli, I. M., Alkislar, M. B., Krothapalli, A., and Lourenco, L. M., "An Experimental Study of Pulsed Jet Ejector," AIAA Paper 2005-1208, Jan. 2005.

[10] Bremhorst, K., and Hollis, P. G., "Velocity Field of an Axisymmetric Pulsed, Subsonic Air Jet," *AIAA Journal*, Vol. 28, No. 12, 1990,

pp. 2043–2049.
[11] Hartmann, J., and Trolle, B., "On a New Method for the Generation of Sound Waves," *Physical Review*, Vol. 20, 1922, pp. 719–727.
[12] Marchese, V. P., Rakowsky, E. L., and Bement, L. J., "A Fluidic Sounding Rocket Motor Ignition System," *Journal of Spacecraft and Rockets*, Vol. 10, No. 11, 1973, pp. 731–734.
[13] Brocher, E., Maresca, C., and Bournay, M.-H., "Fluid Dynamics of the Resonance Tube," *Journal of Fluid Mechanics*, Vol. 43, Pt. 2, 1970, pp. 369–384.
[14] Brun, E., and Boucher, R. M. G., "Research on the Acoustic Air-Jet generator: A New Development," *The Journal of the Acoustical Society of America*, Vol. 29, No. 5, 1957, pp. 573–583.
[15] Sarohia, V., and Back, L. H., "Experimental Investigation of Flow and Heating in a Resonance Tube," *Journal of Fluid Mechanics*, Vol. 94, Pt. 4, 1979, pp. 649–672.
[16] Ackeret, J., "The Role of Entropy in the Aerospace Sciences," *Journal of the Aerospace Sciences*, Vol. 28, No. 2, 1961, pp. 81–102.
[17] Bogdanoff, D. W., "Advanced Injection and Mixing Techniques for Scramjet Combustors," *Journal of Propulsion and Power*, Vol. 10, No. 2, 1994, pp. 183–190.
[18] Kastner, J., and Samimy, M., "Development and Characterization of Hartmann Tube Fluidic Actuators for High-Speed Flow Control," *AIAA Journal*, Vol. 40, No. 10, 2002, pp. 1926–1934.
[19] Brocher, E., "Contribution à l'étude des générateurs acoustique à jet d'air," *Acustica*, Vol. 32, No. 4, 1975, pp. 227–235.
[20] Brocher, E., and Pinna, G., "Aeroacoustical Phenomena in a Horn Excited by a Hartmann-Sprenger Tube," *Acustica*, Vol. 45, No. 3, 1980, pp. 180–189.
[21] Thompson, P. A., "Jet-Driven Resonance Tube," *AIAA Journal*, Vol. 2, No. 7, 1964, pp. 1230–1233.
[22] Payman, W., and Shepherd, W. C. F., "Explosion Waves and Shock Waves 6. The Disturbance Produced by Bursting Diaphragms with Compressed Air," *Proceedings of the Royal Society of London*, Vol. A186, Sept. 1946, pp. 293–321.
[23] Elder, F. K., and de Haas, N., "Experimental Study of the Formation of a Vortex Ring at the Open End of a Cylindrical Shock Tube," *Journal of Applied Physics*, Vol. 23, No. 10, 1952, pp. 1065–1069.
[24] Das, D., Arakeri, J. H., Krothpali, A., and Lourenco, L. M., "Compressible Vortex Ring: A PIV Study," AIAA Paper 2001-2214, May 2001.
[25] Didden, N., "On the Formation of Vortex Rings: Rolling-up and Production of Circulation," *Journal of Applied Mathematics and Physics*, Vol. 30, No. 1, 1979, pp. 101–116.
[26] Maxworthy, T., "The Structure and Stability of Vortex Rings," *Journal of Fluid Mechanics*, Vol. 51, Pt. 1, 1972, pp. 15–32.
[27] Maxworthy, T., "Turbulent Vortex Rings," *Journal of Fluid Mechanics*, Vol. 64, Pt. 2, 1974, pp. 227–239.
[28] Liess, C., and Didden, N., "Experimentelle Untersuchung von Ringwirbeln," *50 Jahre M. P. I. Strömungsforschung, Göttingen, 1925–1975*, Max-Planck-Institut für Strömungsforschung, Göttingen, 1975, pp. 163–173.
[29] Maxworthy, T., "Some Experimental Studies of Vortex Rings," *Journal of Fluid Mechanics*, Vol. 81, Pt. 1, 1977, pp. 465–495.
[30] Gühler, M., and Sallet, D. W., "The Formation of Vortex Rings and Their Initial Motion," *Journal of Flight Sciences and Space Research*, Vol. 3, No. 2, 1979, pp. 109–115.
[31] Willert, C. E., and Gharib, M., "Digital Particle Image Velocimetry," *Experiments in Fluids*, Vol. 10, No. 4, 1991, pp. 181–193.
[32] Johnson, G. M., "An Empirical Model of the Motion of Turbulent Vortex Rings," *AIAA Journal*, Vol. 9, April 1971, pp. 763–764.
[33] Sallet, D. W., and Widmayer, R. S., "An Experimental Investigation of Laminar and Turbulent Vortex Rings in Air," *Journal of Flight Sciences*, Vol. 22, No. 6, 1974, pp. 207–215.
[34] Mohseni, K., and Gharib, M., "A Model for Universal Time Scale of Vortex Ring Formation," *Physics of Fluids*, Vol. 10, No. 10, 1998, pp. 2436–2438.
[35] Saffman, P. G., "On the Formation of Vortex Rings," *Studies in Applied Mathematics*, Vol. 54, No. 4, 1975, pp. 261–268.
[36] Wiegand, A., and Gharib, M., "On the Evolution of Laminar Vortex Rings," *Experiments in Fluids*, Vol. 22, No. 6, 1997, pp. 447–457.
[37] Shariff, K., and Leonard, A., "Vortex Rings," *Annual Review of Fluid Mechanics*, edited by J. L. Lumley, M. Van Dyke, and H. L. Reed, Vol. 24, Annual Reviews, Inc., Palo Alto, CA, 1992, pp. 235–279.
[38] Gharib, M., Rambod, E., and Shariff, K., "A Universal Time Scale for Vortex Ring Formation," *Journal of Fluid Mechanics*, Vol. 360, 1998, pp. 121–140.
[39] Rosenfeld, M., Rambod, E., and Gharib, M., "Circulation and Formation Number of Laminar Vortex Rings," *Journal of Fluid Mechanics*, Vol. 376, 1998, pp. 297–318.
[40] Mohseni, K., Ran, H., and Colonius, T., "Numerical Experiments on Vortex Ring Formation," *Journal of Fluid Mechanics*, Vol. 430, 2001, pp. 267–282.
[41] Krueger, P. S., and Gharib, M., "Thrust Augmentation and Vortex Ring Evolution in a Fully Pulsed Jet," *AIAA Journal*, Vol. 43, No. 4, 2005, pp. 792–801.
[42] Weihs, D., "Periodic Jet Propulsion of Aquatic Creatures," *Fortshritte der Zoologie*, Vol. 24, No. 2/3, 1977, pp. 171–175.
[43] Xia, G., Li, D., and Merkle, C. L., "Effects of a Needle on Hartmann-Sprenger Tube Flows," AIAA Paper 2003-3888, June 2003.
[44] John, W. T., Paxson, D. E., and Wernet, M. P., "Conditionally Sampled Pulsejet Driven Ejector Flow Field Using DPIV," AIAA Paper 2002-3231, June 2002.
[45] Wernet, M. P., "New Insights into PIV Data Using Fuzzy Logic Based Correlation/Particle Tracking Processing," *Experiments in Fluids*, Vol 30, No. 4, 2001, pp. 434–447.
[46] Melling, A., "Tracer Particles and Seeding for Particle Image Velocimetry," *Measurement Science and Technology*, Vol. 8, No. 12, 1997, pp. 1406–1416.
[47] Akhmetov, D. G., "Formation and Basic Parameters of Vortex Rings," *Journal of Applied Mechanics and Technical Physics*, Vol. 42, No. 5, 2001, pp. 794–805.
[48] Sullivan, J. P., Widnall, S. E., and Ezekiel, S., "Study of Vortex Rings Using a Laser Doppler Velocimeter," *AIAA Journal*, Vol. 11, No. 10, 1973, pp. 1384–1389.
[49] Norbury, J., "A Family of Steady Vortex Rings," *Journal of Fluid Mechanics*, Vol. 57, Pt. 3, 1973, pp. 417–431.
[50] Wiegand, A., and Gharib, M., "On the Decay of a Turbulent Vortex Ring," *Physics of Fluids*, Vol. 6, No. 12, 1994, pp. 3806–3808.
[51] Shusser, M., and Gharib, M., "Energy and Velocity of a Forming Vortex Ring," *Physics of Fluids*, Vol. 12, No. 3, 2000, pp. 618–621.
[52] Moore, D. W., "The Effect of Compressibility on the Speed of Propagation of a Vortex Ring," *Proceedings of the Royal Society of London A*, Vol. 397, Jan. 1985, pp. 87–97.
[53] Glezer, A., "The Formation of Vortex Rings," *Physics of Fluids*, Vol. 31, No. 12, 1988, pp. 3532–3541.
[54] Glezer, A., and Coles, D., "An Experimental Study of a Turbulent Vortex Ring," *Journal of Fluid Mechanics*, Vol. 221, 1990, pp. 243–283.
[55] Linden, P. F., and Turner, J. S., "The Formation of 'Optimal' Vortex Rings, and the Efficiency of Propulsion Devices," *Journal of Fluid Mechanics*, Vol. 427, 2001, pp. 61–72.
[56] Fraenkel, L. E., "Examples of Steady Vortex Rings of Small Cross-Section in an Ideal Fluid," *Journal of Fluid Mechanics*, Vol. 51, Pt. 1, 1972, pp. 119–135.
[57] Lamb, S. H., *Hydrodynamics*, Dover, New York, 1932.
[58] Pullin, D. I., "Vortex Ring Formation at Tube and Orifice Openings," *Physics of Fluids*, Vol. 22, No. 3, 1979, pp. 401–403.
[59] Krueger, P. S., "An Over-Pressure Correction to the Slug Model for Vortex Circulation," *Journal of Fluid Mechanics*, Vol. 545, 2005, pp. 427–443.

N. Chokani
Associate Editor